The Astrophysical Journal, 579:327–336, 2002 November 1

ELECTRON PREACCELERATION MECHANISMS IN THE FOOT REGION OF HIGH ALFVÉNIC MACH NUMBER SHOCKS

H. Schmitz and S. C. Chapman
Space and Astrophysics Group, Department of Physics, University of Warwick, Coventry CV4 7AL, UK;
holgers@astro.warwick.ac.uk

and

R. O. Dendy
UKAEA Fusion, Culham Science Centre, Abingdon, Oxfordshire OX14 3DB, UK
Received 2002 February 15; accepted 2002 May 10

ABSTRACT

High Mach number, collisionless perpendicular shocks are known to accelerate electrons to strongly relativistic energies by diffusive shock acceleration. This presupposes the existence of mildly relativistic electrons, whose preacceleration mechanism from lower ambient energies (the injection problem) remains an open question. Here a particle in cell simulation is used to investigate the preacceleration mechanism. Depending on the parameters of the upstream plasma and the shock velocity, the growth rate of instabilities in the foot of the shock can be significant, leading to the existence of nonlinear modes and the formation of electron phase space holes. It is found that these are associated with electron preacceleration, which can be divided into three phases. In the initial phase electrons are accelerated in the shock foot by the surfatron mechanism, which involves particle trapping in nonlinear wave modes. This mechanism is strongly linked to the existence of solitary electron phase space holes. The second phase is characterized by fluctuations in the magnetic field strength together with μ-conserving motion of the electrons. Finally, in the third phase the magnetic moment μ is no longer conserved, perhaps due to turbulent scattering processes. Energies up to Lorentz factors of $\simeq 6$ are achieved, for simulations in which the inflow kinetic energy of upstream electrons is 3.5 keV.

Subject headings: acceleration of particles — MHD — shock waves — supernovae: general

1. INTRODUCTION

Observations of supernova remnants (SNRs) show that these objects are a strong source of radio synchrotron emission, indicating the presence of highly energetic electrons (Biermann & Cassinelli 1993). Synchrotron emission even up to X-ray wavelengths has been observed (Pohl & Esposito 1998), corresponding to electron energies up to 10^{14} eV. Higher resolution measurements (Koyama, Petre, & Gotthelf 1995) show that the highest energies are found at the rim, leading to the conclusion that electrons are accelerated in the shock created by the super-Alfvénic SNR ejecta propagating into the interstellar medium.

There are several mechanisms that can accelerate particles in collisionless perpendicular shocks. The simplest of these is shock drift acceleration, where the gradient in magnetic field strength causes electrons to drift parallel to the shock front. Here they can be accelerated by the electric field $\boldsymbol{u}_{\rm shock} \times \boldsymbol{B}_1$ arising from the motion of the shock with velocity $\boldsymbol{u}_{\rm shock}$ through an undisturbed plasma with magnetic field $\boldsymbol{B}_1$ in the shock frame of reference. The electrons thus form a high-velocity electron beam. Drift acceleration can have high efficiency since all electrons that pass through the shock can be accelerated by it, irrespective of their velocity. However, it is limited insofar as the electrons encounter the shock only for a finite time. Thus, unless there is a mechanism causing the electrons to encounter the shock front repeatedly, there is an upper limit on the energy.

First-order Fermi acceleration results from particles repeatedly crossing the shock, being reflected by turbulence-generated coherent structures that are embedded in the upstream and downstream flows. While the presence of such structures in the downstream region is expected, Bell (1978) showed that even the initially undisturbed upstream region will exhibit fluctuations that are induced by the accelerated particles themselves. Thus, by repeatedly crossing the shock front and scattering off the comoving turbulence structures in the two converging flows, the electrons will be accelerated. In perpendicular shocks, however, the particles at background temperature cannot move freely along the shock normal because of the magnetic field. This means that particles must be preaccelerated, so that the Larmor radius becomes large compared to the mean free path for scattering off the coherent structures, if first-order Fermi acceleration is to remain possible (Jokipii 1987).

In second-order Fermi acceleration, particles scatter off magnetic fluctuations on the same (downstream) side of the shock. These fluctuations have a random velocity component with respect to the average flow velocity. A particle scattering on these fluctuations can be accelerated in a head on collision or decelerated in a retreating collision. To first order, therefore, particles are not accelerated. A second-order effect is that, on average, there are more head-on collisions than retreating ones, and due to this the particles are accelerated. This mechanism works at both parallel and perpendicular shocks; however, it is much less efficient than first-order Fermi acceleration. First- and second-order Fermi acceleration are often referred to as diffusive shock acceleration (Giacalone et al. 1993).

It follows that diffusive shock acceleration can only efficiently accelerate electrons in perpendicular shocks if they already have high energy compared to the background thermal energy, that is if they are mildly relativistic. The nature of the preacceleration mechanism (the "injection" prob-

lem) still remains an open question (Levinson 1997). In a perpendicular shock, ions are reflected off the shock front, thus creating the foot of the shock. This foot has three ion populations: (a) the inflowing undisturbed upstream ions, and the reflected ions (b) flowing in the opposite direction and then (c) gyrating back into the downstream region. Papadopoulos (1988) proposed that instabilities caused by the two counter-streaming ion populations of inflowing and reflected ions could produce the necessary electron acceleration. These ion beams are Buneman unstable if their relative velocity $u_{\rm rel}$ is greater than the thermal velocity $v_{e,\rm th}$ of the electrons (Buneman 1958). Assuming that $u_{\rm rel} = 2u_1$, where u_1 is the upstream or equivalently the shock velocity, this condition can be written as

$$2\frac{M_{\rm A}}{\beta}\frac{m}{M} > 1 \ . \tag{1}$$

Here $M_{\rm A}$ is the Alfvénic Mach number of the shock, β is the local ratio of kinetic to magnetic pressure, and m and M are the electron and ion rest masses. Waves generated by the Buneman instability can heat electrons rapidly on the timescale of the electron plasma frequency and could contribute to the preacceleration of the electrons (Papadopoulos 1988). This was confirmed with a particle in cell simulation by Dieckmann et al. (2000), in which the initial conditions were chosen to represent the local conditions in the shock foot. A number of hybrid simulations have been carried out to investigate this question (see, e.g., Cargill & Papadopoulos 1988, Giacalone et al. 1993, or Burgess, Wilkinson, & Schwartz 1989); however, these typically assume a thermal electron distribution and cannot account for nonthermal electron heating or acceleration. Shimada & Hoshino (2000) simulated a high Mach number perpendicular shock with a fully kinetic particle in cell code. They showed that preacceleration depends on the Mach number of the shock. At high Mach numbers the time-dependent behavior of the shock changes, characteristic electron phase space holes appear in the foot of the shock and the downstream electron distribution function shows a high-energy tail. Recently, Schmitz, Chapman, & Dendy (2002) demonstrated that all these effects depend not only on the Mach number, but also on the upstream plasma β, the ratio between thermal pressure and magnetic pressure. The results of the particle in cell simulations of both Shimada & Hoshino (2000) and Schmitz et al. (2002) suggest a strong link between the existence of the electron holes and the high-energy tail of the downstream electron distribution. The details of the underlying mechanism have, however, not yet been investigated. McClements et al. (2001) proposed that surfatron acceleration might be responsible for electron acceleration in perpendicular high Mach number shocks. In this mechanism, which was brought forward by Katsouleas & Dawson (1983) as a method of particle acceleration through laser-plasma interaction, electrons are trapped in a wave field propagating perpendicular to the magnetic field lines.

It is the aim of this paper to investigate the electron acceleration mechanism and to verify the importance of the surfatron mechanism. We have performed a series of particle in cell simulations designed to investigate the mechanism by which the fastest electrons gain their energy. The link between the electron phase space holes and the preacceleration is confirmed, and distinct phases in the electron acceleration are distinguished.

Hoshino & Shimada (2002) very recently published results for a similar configuration that also confirm the link between the existence of electrostatic solitary waves and the preacceleration of electrons. In the present paper we investigate in detail the trapping and detrapping mechanisms, and the maximum achievable energies for the electrons.

2. SIMULATION

The electron acceleration takes place in a region of the shock that is far from equilibrium, both for the ions and for the electrons. This makes a fully kinetic description necessary. To this end we use a relativistic electromagnetic particle in cell (PIC) code. In this simulation technique the distribution functions of ions and electrons are represented by a large number of simulation particles. Every simulation particle is described by a space coordinate and a velocity. The currents and the electromagnetic fields are given on a grid in configuration space. Details of the PIC simulation technique can be found in Hockney & Eastwood (1981). In this investigation we use the same PIC code (Devine, Chapman, & Eastwood 1995) that we used in a recent study of the injection problem (Schmitz et al. 2002). Similar relativistic electromagnetic PIC codes have been used previously to investigate acceleration processes in astrophysical plasmas; see, e.g., Hoshino et al. (1992), Bessho & Ohsawa (1999), or Shimada & Hoshino (2000).

We consider the same geometry as used by Schmitz et al. (2002). The simulation is one-dimensional in space along the x-axis, while retaining all three velocity components ($1x3v$). The piston method (Burgess et al. 1989 and references therein) is used to set up the shock. Electrons and ions are injected on the left side of the simulation box, while the right boundary is taken to be completely reflecting and perfectly conducting. Incoming particles and reflected particles will then create a plasma at rest at the right, eventually forming a shock that will travel toward the left. After some time the shock would reach the left boundary of the system: however, in order to simulate the shock for a longer period of time without increasing the size of the simulation box, we implement the simple shock following algorithm described in Schmitz et al. (2002).

We simulate a purely perpendicular shock with the upstream magnetic field lying in the z-direction. The value of the upstream magnetic field was chosen to be $B_{z,1} = 10^{-7}$ tesla, which is consistent with values expected at supernova remnants (Ellison & Reynolds 1991). The plasma is made up of electrons and protons and assuming quasineutrality it follows that $n_e = n_i = n$. The electrons and ions are assumed to have the same upstream temperature $T_{i,1} = T_{e,1} \equiv T_1$, resulting in the same value of the plasma β,

$$\beta_k = \frac{nk_B T_{k,1}}{B_{z,1}^2/2\mu_0} \ , \qquad k = i, e \ , \tag{2}$$

for both species, $\beta_e = \beta_i = \beta = 0.15$. The shock has an Alfvénic Mach number of 10.5, and the upstream ratio of electron plasma frequency to electron gyro frequency is $\omega_{pe}/\omega_{ce} = 20$. The simulation box consists of 15,000 grid cells, each of the size of one Debye length. The total size of the system corresponds to about 28 ion Larmor radii λ_{ci}, calculated using the upstream magnetic field $B_{z,1}$ and the shock velocity u_1. A reduced ratio of ion to electron mass $M/m = 20$ has been adopted. This choice of values has

previously been shown to produce a nonthermal downstream electron distribution with a high-energy tail (Shimada & Hoshino 2000 and Schmitz et al. 2002).

3. RESULTS

As shown in Schmitz et al. (2002) and Shimada & Hoshino (2000), a shock with the above parameters exhibits strongly time-dependent behavior. Shock formation and evolution is typically characterized by the length scale given by the ion Larmor radius λ_{ci}. Conversely, where electron dynamics are important, a characteristic length scale is given by the electron inertial length c/ω_{pe}. The normalization of spatial coordinates in our figures is carried out using one or the other of these parameters as appropriate. As shown in Figure 1, ions are reflected at the shock front and form the foot of the shock. A large electron phase space hole (EPH) forms at $x/\lambda_{ci} = 1.6$, which is located, as we shall see, at the turnaround position of the reflected ions. Within the shock foot, further electron phase space holes can be seen; this is consistent with Buneman instability between the reflected ions and the incoming electrons (Hoshino & Shimada 2002 and references therein). For those parameters in which the shock foot exhibits strong instabilities and EPHs, the downstream electron energy distribution deviates significantly from a pure thermal distribution, with a fast electron population. This was shown by Schmitz et al. (2002) and Shimada & Hoshino (2000), who also showed that in the opposite case, where no EPHs were observed, the downstream electron energy distribution can be well described by a Maxwellian. There consequently appears to be a strong link between the existence of EPHs and a fast downstream electron population.

To investigate the acceleration mechanism and the role of the electron phase space holes therein, we run the simulation, calculating the downstream energies for every electron and keeping track of which particles achieve the highest downstream energies. Repeating the simulation with identical parameters and identical initial conditions, we then follow the 10 fastest electrons through the simulation from the time they enter the box at the left boundary.

Figure 2 traces the position versus time for two of these electrons in the shock rest frame. For future reference we label these electrons A and B, and these plots are superimposed on a gray-scale display of the computed spatiotemporal evolution of the magnetic field. The particles enter the simulation box at the left with the upstream flow velocity $u_{\rm flow}$. This high velocity is indicated by the small slope of the curves in this region. The different times at which the electrons enter the box can be seen by the offset of the curves on the vertical time axis. When the electrons encounter the foot of the shock at about $x = 9\lambda_{ci}$ they are suddenly decelerated in the x-direction and remain almost at rest with respect to the shock for about one electron cyclotron period. Thereafter, the electrons start gyrating and are then convected downstream with the magnetic field lines.

The gyration with large gyroradii immediately after encountering the foot of the shock indicates that the electrons must have gained perpendicular energy during the small time interval in which they appear to be resting in the foot region. In Figure 3 we plot the kinetic energy of the two particles versus their position in the shock. The kinetic energy $E_{\rm kin}$ is calculated in the rest frame of the shock. For this reason the inflowing particles show a periodic oscillation in their energies due to their cycloidal motion in the upstream magnetic field; they have constant energy in the upstream rest frame. A striking feature in this diagram is the sharp increase at about $x = 9\lambda_{ci}$ coinciding with the position of electron p_x-deceleration, shown as almost vertical lines in Figure 2. The increase of energy is by roughly a

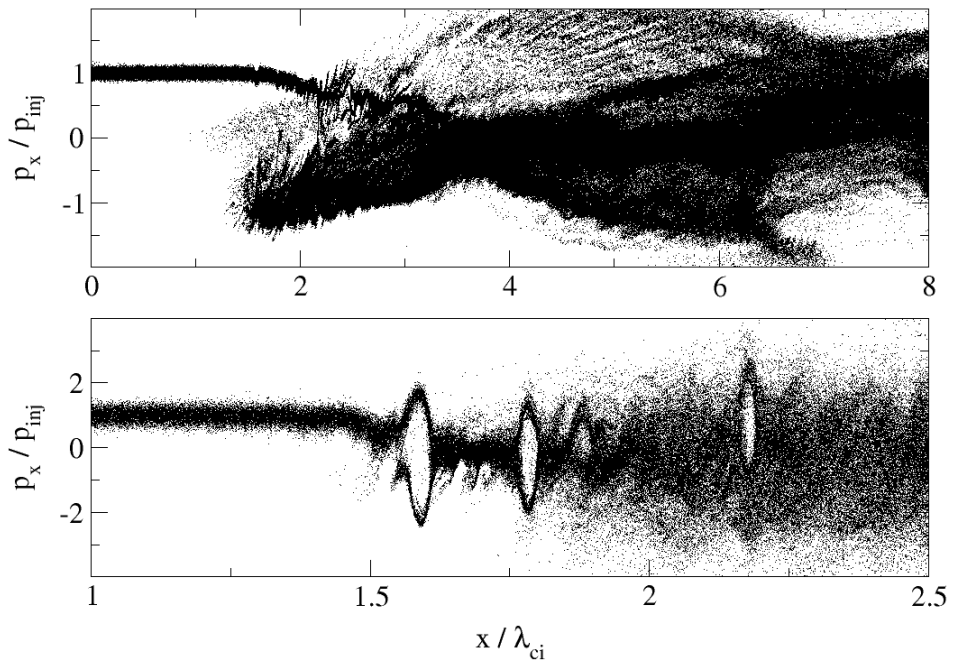

FIG. 1.—Ion phase space distribution (*upper panel*), and the electron phase space distribution (*lower panel*), at $t\omega_{ci} \approx 2.5$. The particle inflow is from the left, and the right boundary is situated far right of this plot at $x/\lambda_{ci} \approx 25$. The frame of reference is the downstream rest frame. The ion phase space plot shows a large portion of the simulation box, while the electron phase space plot focuses on the foot region.

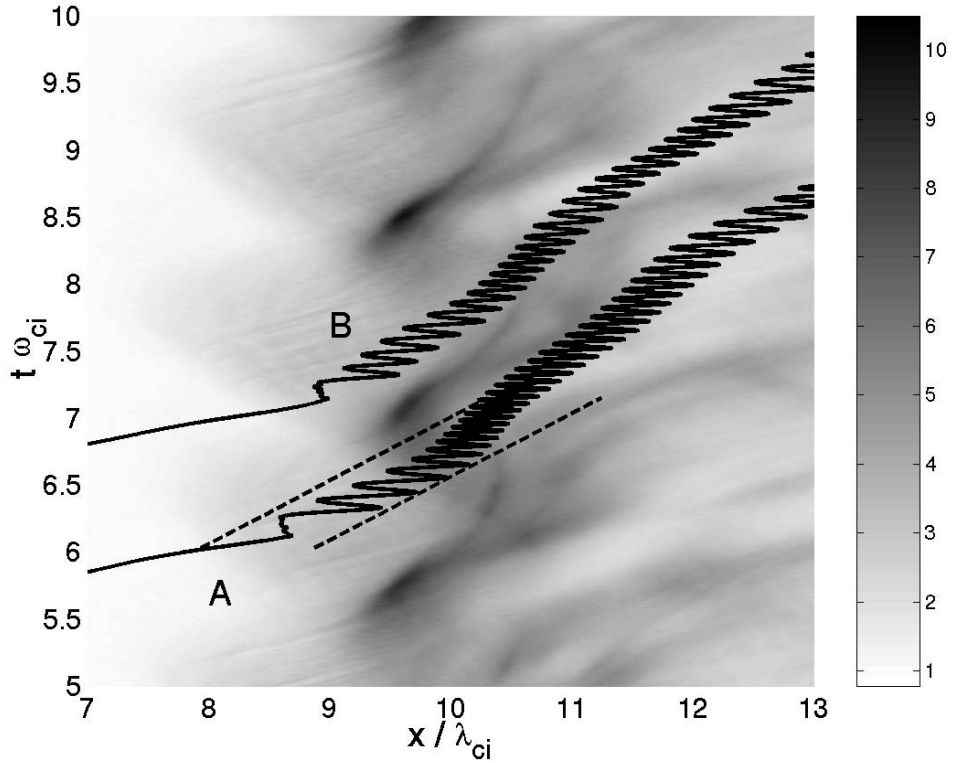

FIG. 2.—Magnetic field component B_z vs. x and t, coded as gray-scale plot. On top of this, the x-positions of two sample electrons vs. time are plotted as solid lines. The electrons move in from the left with a high directed velocity. When they enter the foot of the shock, they are strongly decelerated in the x-direction. After a short time in which they appear not to move at all, they start gyrating and convect downstream. The electrons are marked A and B for future reference.

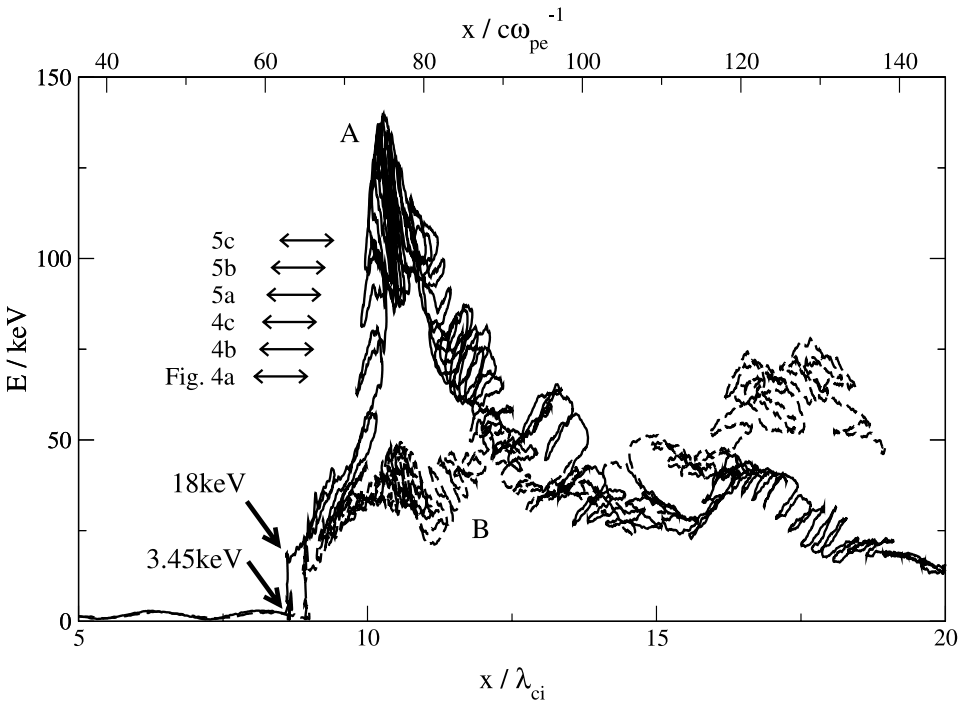

FIG. 3.—Energies of the electrons A and B vs. their x-position as they travel through the shock from left to right. An initial fast acceleration in the foot of the shock and a following phase of slow energy change can be distinguished. The energies at the beginning and end of the initial fast acceleration for electron A are shown. The regions plotted in the phase space diagrams of Figs. 5 and 6 are shown by the double arrows.

factor of 20, and it takes place during a single electron cyclotron period. It follows that a highly nonadiabatic phenomenon must be responsible for the acceleration.

After this initial acceleration the electron energy still evolves, but the changes are on a much longer timescale. This means that adiabatic effects may be responsible for these later changes in electron energy. The energy of electron A in Figure 3 rises almost to 200 keV, which is more than $55E_1$, where $E_1 = mu_1/2$ is the upstream flow kinetic energy per electron in the shock frame. This maximum is reached at $x \approx 10.5\lambda_{ci}$, which corresponds to the position of the magnetic field overshoot of the shock, see Figure 3. The energy then declines until at $x = 20\lambda_{ci}$ it has dropped below the level reached after the initial acceleration. For comparison, the x-component of this electron's momentum during this acceleration phase is plotted in Figure 4: here the points corresponding to the plots in Figures 5 and 6, described below, are marked by the corresponding time. In contrast electron B shows slowly increasing energy for the rest of the simulation time. Its final energy is approximately a factor of 2 above the initial acceleration energy. Multiple scattering of both A and B is thus occurring in both the overshoot and the downstream regions.

We have seen that those electrons that emerge as the highest energy electrons downstream have initially undergone a fast and strongly nonadiabatic acceleration phase in the foot of the shock. Later, when the electrons pass through the shock into the downstream region, they undergo repeated scattering; their energy changes and can on the whole be increased, although on a much longer timescale. This behavior is found for all of the 10 sample electrons that we follow through the shock. To investigate the initial acceleration further we rerun the simulation. This time, for every sampled electron we define a window in the space coordinate x comoving with the average velocity of the particle during its time of acceleration. The size of the window is chosen so that the particle always lies inside. We then plot the distributions of electrons and ions in phase space inside this window, creating a time series of plots with the sample particle lying inside. An example of the boundaries of a comoving window is shown by the dashed lines in Figure 2.

Figures 5 and 6 show these phase space plots for the particle A. The left panel of each subplot in Figures 5 and 6 represents the electron distribution in phase space, while the right panel represents the ion distribution in phase space. The sample electron is denoted by the small black dot in the electron phase space plots. Note that these figures do not encompass the whole shock, but only a small region extending over less than one ion Larmor radius. In the first row of Figure 5 we see the narrow upstream beam of ions flowing in from the left with positive momenta p_x. At the right of the ion phase space plot a population with negative p_x and a larger thermal spread is visible. This is the ion population that is reflected at the shock and forms the shock foot. This figure thus shows only the very leftmost (i.e., upstream) part of the foot of the shock. The electron phase space distribution in the same region is more highly structured. Just at the position where the first reflected ions appear, an electron phase space hole (EPH) is seen to form. To the right of this hole the electron phase space shows some irregular structure; at far right the irregularities grow, and here also some disturbance of the inflowing ion beam is visible. As we shall see, these disturbances in the ion beam accompany the formation and growth of the electron phase space hole. Thus far, the sample electron is still in the undisturbed region just about to encounter the EPH, but in the plots in the second

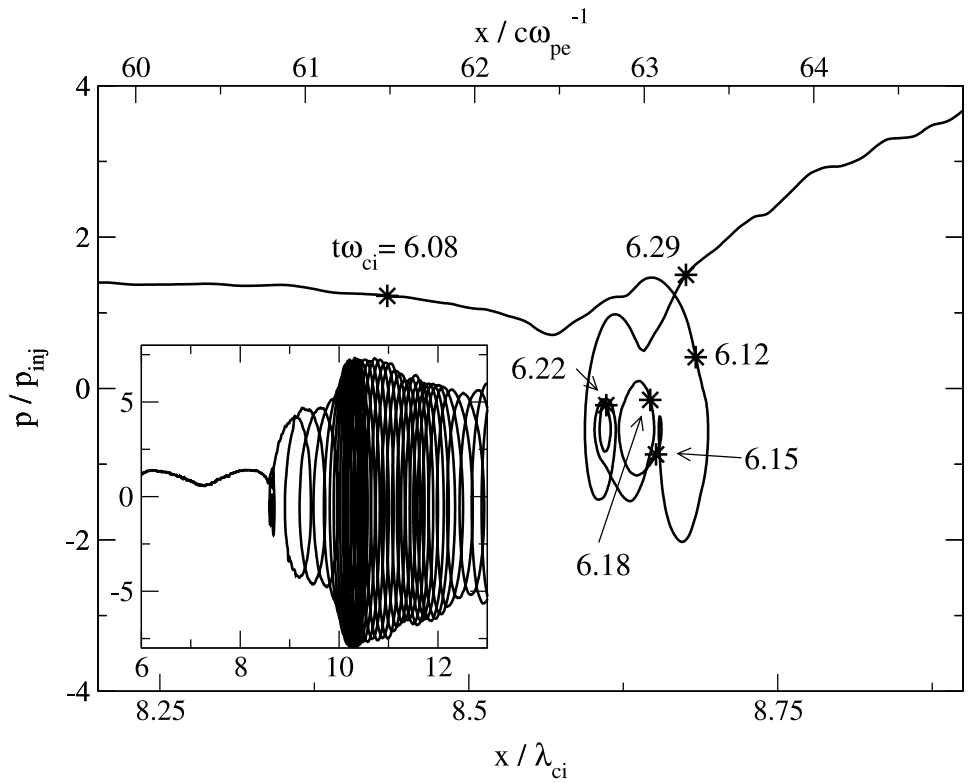

FIG. 4.—x-component of the momentum of electron A vs. its position x during the fast acceleration phase. The points at which the phase space plots in Figs. 5 and 6 are taken are marked by their corresponding times. The inset shows the same plot over a greater range.

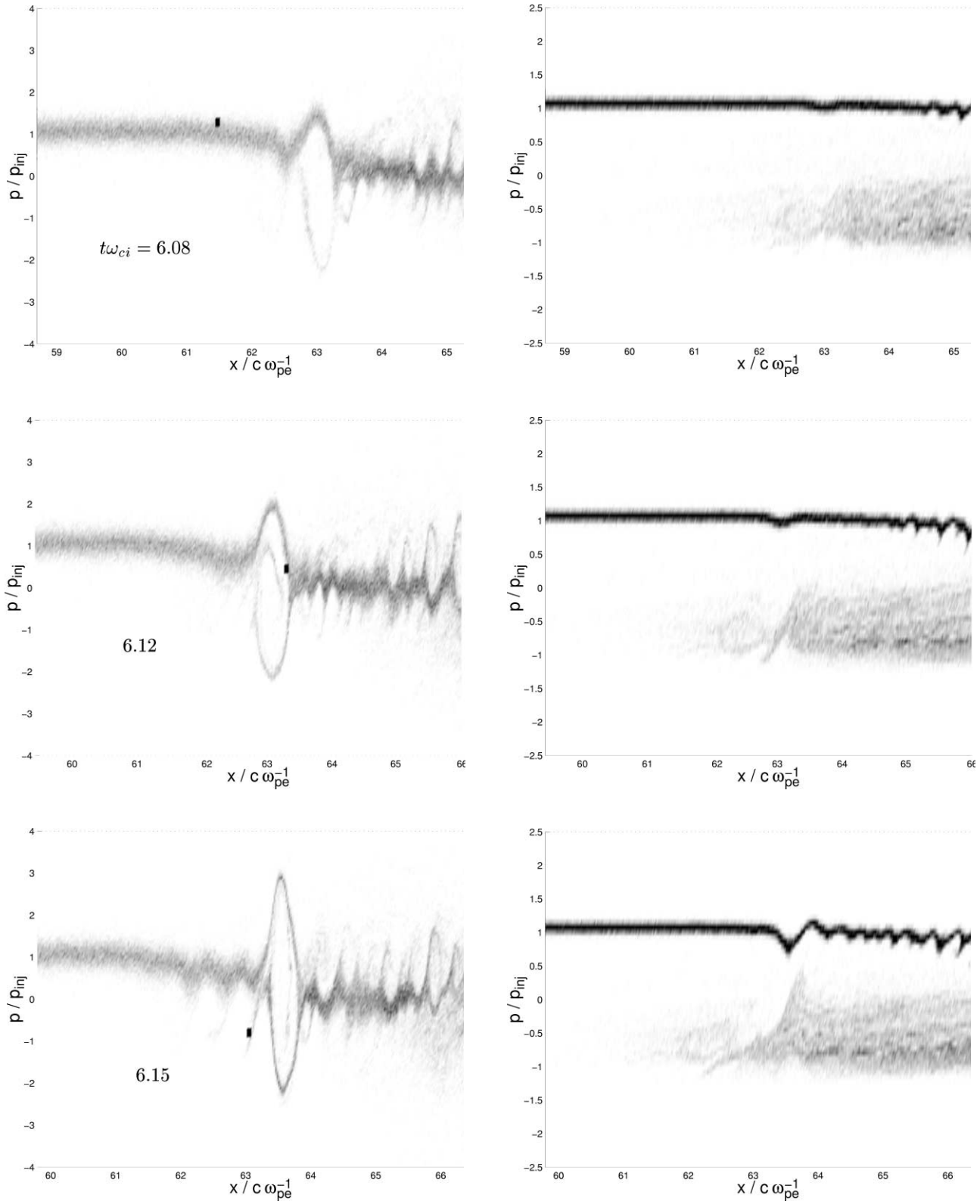

FIG. 5.—Particle distributions in phase space near the location of sample electron A. The left column shows the electron distribution in p_x-x phase space at different times. The sample electron is indicated by the black dot. The right column shows the ion distribution in phase space at the same times. The frame of the images moves right with time following the average motion of the particle as indicated by the dashed lines in Fig. 2. The top row is for $t \approx 6.08\omega_{ci}$, the middle for $t \approx 6.12\omega_{ci}$, and the bottom for $t \approx 6.15\omega_{ci}$.

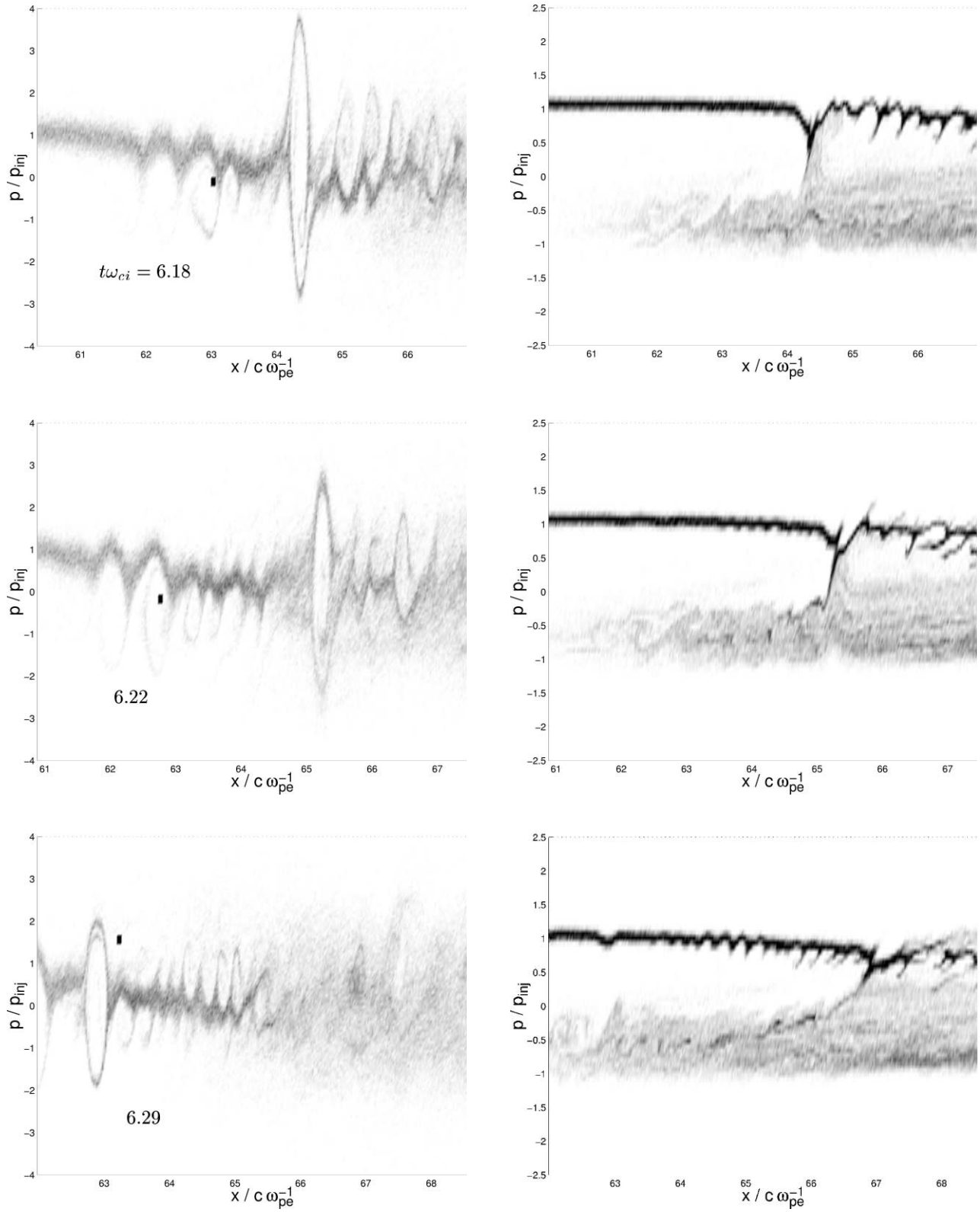

FIG. 6.—Same as Fig. 5: particle distributions in phase space near the location of sample electron A, at later times $t \approx 6.18\omega_{ci}$ (*top*), $t \approx 6.22\omega_{ci}$ (*middle*), and $t \approx 6.29\omega_{ci}$ (*bottom*).

row of Figure 5 the sample electron has entered the EPH, which has grown in size by a small amount. The electron is reflected at the right side of the EPH and, in the plots in the third row at the time $t \approx 6.15\omega_{ci}$, it leaves the now completely formed EPH toward the left, where a new EPH is just beginning to form. At the position of the existing EPH, which is now quite large, there is a small structure in the incoming ion beam. This indicates the existence of a coupled electron phase space hole–ion Langmuir soliton (EPH-LS); such structures have been described by Saeki & Rasmussen

(1991). The EPH, which can be regarded as a vortex in the phase space fluid, can propagate at arbitrary velocity, depending on the initial conditions (Berk & Roberts 1967; Saeki et al. 1979). In contrast, the propagation speed of an ion Langmuir soliton is determined uniquely by its amplitude (Kako & Yajima 1980) and is of the order of the ion acoustic speed. Saeki & Rasmussen (1991) showed that the coupled EPS-LS state, although faster than the pure LS, can only propagate at fixed velocities, depending on the amplitude of the soliton and the number of trapped electrons in the phase space hole. These velocities are still of the order of a few times the ion acoustic velocity, which is small compared to $u_{\rm flow}$. This means that the whole structure is effectively convected along with the cold inflowing ion beam. At the same time the sample electron is on average at rest with respect to the shock rest frame. This means that it moves toward the left in the comoving series of plots, as seen in the first row of Figure 6. A second EPH develops around the sample electron, which remains electrostatically trapped in the growing structure. At the later time $t \approx 6.22\omega_{ci}$ (Fig. 6, *second row*), the new EPH has grown and still confines the sample electron. As the hole structure grows, it too creates a coupled EPH-LS. This causes a change in the velocity of the structure toward the downstream direction, which is seen in the bottom row of Figure 6. This change in velocity enables the electron to escape. While trapped in the forming EPH, the electrons energy rose from about 3.45 to 35 keV. The points referring to the trapping, at $t \approx 6.15\omega_{ci}$, and untrapping, just after $t \approx 6.22\omega_{ci}$, are marked in Figure 3.

The electrons gain their energy while being nonlinearly trapped in a solitary wave structure. There are thus points of contact with the proposal by McClements et al. (2001) that surfatron acceleration might be responsible for electron acceleration in perpendicular high Mach number shocks. As described before, in this mechanism electrons are trapped in a wave field propagating perpendicular to the magnetic field lines. In the zero phase velocity frame of reference there is an electric field $E_y = v_{\rm ph} B_z$, assuming that the phase velocity $v_{\rm ph}$ is in the x-direction and the magnetic field points in the z-direction. This electric field can accelerate the electrons as long as they remain trapped in the potential trough of the wave. McClements et al. (2001) considered an infinitely extended periodic wave train, where electrons can untrap and then be retrapped in another potential minimum travelling at the same speed. This can lead to repeated acceleration and thus in principle to unlimited gains in particle energy. In our more realistic simulation of the shock, the situation in the foot turns out to be somewhat different. Instead of an infinitely extended wave field we observe solitary waves with different velocities. The foot of the shock repeatedly reforms and disappears again. EPH structures form repeatedly at the leading edge of the reforming foot and, as they grow into EPH-LS structures, they are naturally convected downstream with the relatively cold inflowing ion beam. With the collapse of the shock, the electron phase space holes disappear, and the electrons are freely convected downstream without the possibility of acceleration by an EPH. Thus, there is a limited time in which the electrons can interact with the EPH structures, and our simulations show that this time is approximately equal to the ion cyclotron period ω_{ci}^{-1}. Although brief, this is still enough to achieve the energies observed in the simulation. To see how this is possible, let us now investigate the temporal behavior of the relativistic momentum component

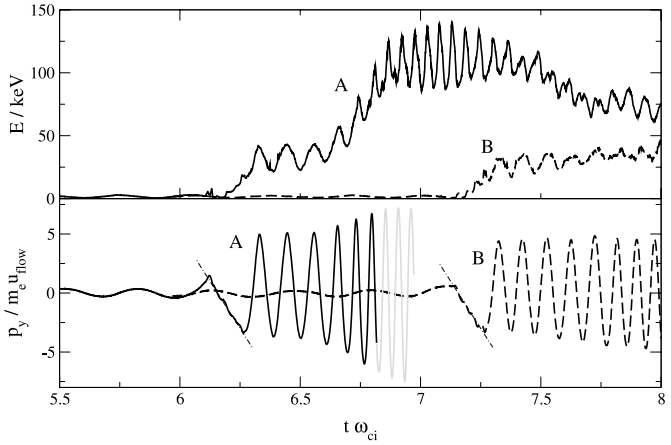

FIG. 7.—Lower panel shows the v_y-velocity of the electrons A and B vs. time as they travel through the shock. Upper panel shows their energy vs. time. During the initial fast acceleration phase, v_y changes almost linearly with time, indicating constant acceleration. The linear regression curves for these intervals are shown by the dot-dashed lines.

p_y, which is perpendicular to the shock normal and to the upstream magnetic field lines. Figure 7 shows p_y versus time in the lower panel, and relativistic kinetic energy $E_{\rm kin} = (\gamma - 1)m_e c^2$ in the upper panel, for the particles A and B. The time interval is chosen so that the trapping time for the two electrons is clearly visible. Electron A is trapped from $t \approx 6.1\omega_{ci}$ to $t \approx 6.25\omega_{ci}$, whereas electron B is trapped from $t \approx 7.14\omega_{ci}$ to $t \approx 7.27\omega_{ci}$. In both cases, it is clearly visible that p_y changes almost linearly for as long as the electrons remain trapped. This indicates acceleration by the surfatron mechanism. To get an estimate of the average electric field E_y seen by the particle, we measure the slope of the linear acceleration interval of p_y and find that for the two electrons $\dot{p_y} \approx 33$–$35 m u_{\rm flow}\omega_{ci}$. This corresponds to an average electric field $\langle E_y \rangle \approx 1.75 u_{\rm shock} B_{z,1} = 1.75 E_{y,1}$; thus, the upstream electric field in the shock rest frame is enhanced by a factor of 1.75, which arises from the increase of magnetic field strength in the shock foot region. Thus, we conclude that the surfatron mechanism is indeed responsible for the initial fast electron acceleration, which is strongly nonadiabatic. Furthermore, given the acceleration rate for p_y together with the estimate of the maximum acceleration time of ω_{ci}^{-1}, we find that the maximum gain in momentum is given by 33–$35 m u_{\rm flow}$, which corresponds to an energy gain factor of approximately 10^3. Given an inflow energy of about 3.5 keV per electron the maximum energy achievable by this mechanism is 3.5 MeV. This corresponds to a maximum electron Lorentz factor in excess of 6, so that mildly relativistic electrons can indeed be generated by this mechanism.

Now let us consider the mechanism responsible for the slow change in the energy of electrons that occurs in our simulation after they have been preaccelerated by the surfatron mechanism. As mentioned before, these changes take place on a much longer timescale than the electron gyration period and could therefore be due to adiabatic particle motion. To investigate this, we plot the magnetic moment $\mu = m v_\perp / 2B$ as a function of time for both particles A and B in the bottom panel of Figure 8. As in Figure 7, the top panel shows the evolution of kinetic energy with time. The sudden increase of μ during the fast acceleration phase

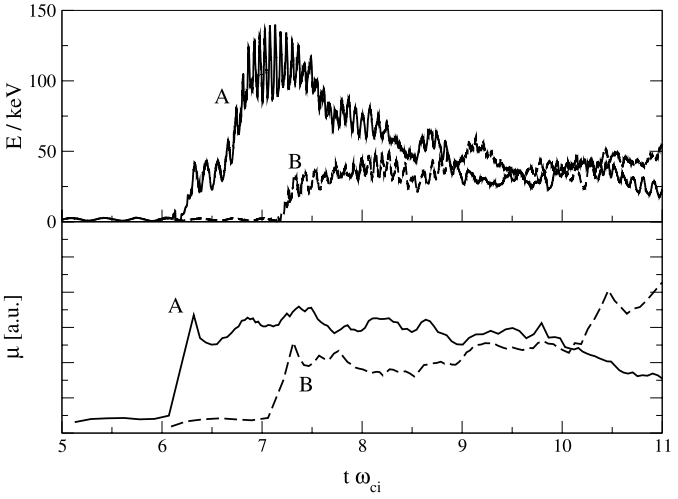

FIG. 8.—Lower panel shows the magnetic moment μ of the electrons A and B vs. time as they travel through the shock. Upper panel shows their energy vs. time. During the initial fast acceleration phase, μ changes rapidly, but it stays approximately constant afterward although the energies change. Only in the downstream region at far right of the simulation box does μ change again.

underlines the strong nonadiabaticity of surfatron acceleration. After this phase the magnetic moment stays approximately constant for approximately 20 electron gyroperiods. In contrast, the particles energies, especially that of electron A, change dramatically during this time. The conservation of μ suggests that these changes are simply due to fluctuations in magnetic field strength combined with adiabatic particle motion. This means that the kinetic energy varies in proportion to the magnitude of the magnetic field, which further implies that the overall effect of this second phase mechanism on the energy cannot exceed the ratio of magnetic field strength in the downstream region to that in the shock foot, where the onset of adiabatic motion lies.

Finally, looking at the far right of Figure 8 we identify a third phase during which the magnetic moment can change in the downstream region. While it decreases slowly for electron A, there is a clearly visible increase of μ for electron B. This indicates the existence of a further mechanism that can slowly change the electron energy in a nonadiabatic way. Due to the limitations on the size of the simulation box and the maximum simulation time, no diagnostics of this third phase of the acceleration were performed. Thus, we can only speculate about the underlying mechanism, which might be due to turbulent scattering.

4. CONCLUSIONS

We have investigated the acceleration of electrons in high Alfvénic Mach number perpendicular shocks by following sample electrons that are known to be accelerated to high energies in a fully kinetic relativistic PIC simulation. Their dynamical evolution in terms of position, velocity, and energy has been observed and analyzed.

The electron acceleration takes place in three phases. When the sample electrons first encounter the foot of the shock, they undergo an initial fast acceleration which can be understood in terms of the surfatron mechanism. This involves acceleration of particles trapped in the potential troughs of nonlinear waves travelling perpendicular to the magnetic field. The trapped particles see an electric field that is present in the zero phase velocity frame of reference of the wave. This electric field can accelerate the particles in the direction that is perpendicular to both the shock normal and to the magnetic field lines. In contrast to earlier investigations, it was found that the electrons are trapped in solitary electron phase space hole structures, instead of an infinitely extended wave train. The electrons can only interact with the electron phase space holes for a finite time, which places a fundamental constraint on the energies achievable. The highest energies observed in the simulation at the end of this initial acceleration phase were about 40–50 keV. This is limited by the finite number of particles in the simulation; in principle, as we have seen, our results imply that electrons could be accelerated in this way to energies as high as $\approx$3.5 MeV.

In the second acceleration phase, the electron energies change slowly in response to changes in local magnetic field strength combined with adiabatic μ-conserving particle motion. During this phase the electron energy can undergo substantial changes; however, the overall increase is limited by the ratio of the magnetic field strength in the downstream region to that at the shock foot, where the onset of adiabatic motion lies.

Finally, the electrons can undergo further nonadiabatic acceleration or deceleration. The nature of this last mechanism could, however, not be identified due to lack of data and limitations in the size of the simulation box, and it remains an open question for further investigations.

In conclusion, we have shown that electrons can be accelerated to mildly relativistic energies in perpendicular high Alfvénic Mach number magnetosonic shocks. The most important physical process identified is the surfatron mechanism, which was proposed by McClements et al. (2001) to be responsible for cosmic-ray electron preacceleration. Assuming repeated trapping and untrapping for the duration of a shock foot formation cycle, electrons could be accelerated to Lorentz factors in excess of 6, and this would then allow them to be further accelerated by Fermi acceleration. Together with the results of other recent papers (Dieckmann et al. 2000; Shimada & Hoshino 2000; McClements et al. 2001; Hoshino & Shimada 2002; Schmitz et al. 2002), the present results suggest that a solution for the classical injection problem for cosmic-ray electrons is now emerging.

This work was supported in part by the Commission of the European Communities under TMR Astroplasmaphysics Network Contract ERB-CHRXCT980168. S. C. C. acknowledges PPARC, and R. O. D. support from the UK DTI. We are grateful to K. G. McClements for helpful comments.

REFERENCES

Bell, A. R. 1978, MNRAS, 182, 147
Berk, H. L., & Roberts, K. V. 1967, Phys. Fluids, 10, 1595
Bessho, N., & Ohsawa, Y. 1999, Phys. Plasmas, 6, 3076
Biermann, P. L., & Cassinelli, J. P. 1993, A&A, 277, 691
Buneman, O. 1958, Phys. Rev. Lett., 1, 8
Burgess, D., Wilkinson, W. P., & Schwartz, S. J. 1989, J. Geophys. Res., 94, 8783
Cargill, P. J., & Papadopoulos, K. 1988, ApJ, 329, L29
Devine, P. E., Chapman, S. C., & Eastwood, J. W. 1995, J. Geophys. Res., 100, 17189

Dieckmann, M. E., McClements, K. G., Chapman, S. C., Dendy, R. O., & Drury, L. O'C. 2000, A&A, 356, 377
Ellison, D. C., & Reynolds, S. P. 1991, ApJ, 382, 242
Giacalone, J., Burgess, D., Schwartz, S., & Ellison, D. 1993, ApJ, 402, 550
Hockney, R. W., & Eastwood, J. W. 1981, Computer Simulations Using Particles (New York: McGraw Hill)
Hoshino, M., Arons, J., Gallant, Y. A., & Langdon, A. B. 1992, ApJ, 390, 454
Hoshino, M., & Shimada, N. 2002, ApJ, 572, 880
Jokipii, J. R. 1987, ApJ, 313, 842
Kako, F., & Yajima, N. 1980, J. Phys. Soc. Japan, 49, 2063
Katsouleas, T., & Dawson, J. M. 1983, Phys. Rev. Lett., 30, 3241
Koyama, K., Petre, R., & Gotthelf, E. V. 1995, Nature, 378, 255
Levinson, A. 1997, MNRAS, 278, 1018
McClements, K. G., Dieckmann, M. E., Ynnerman, A., Chapman, S. C., & Dendy, R. O. 2001, Phys. Rev. Lett., 87, 255002
Papadopoulos, K. 1988, Ap&SS, 144, 535
Pohl, M., & Esposito, J. A. 1998, ApJ, 507, 327
Saeki, K., Michelsen, P., Pecseli, H. L., & Rasmussen, J. J. 1979, Phys. Rev. Lett., 42, 501
Saeki, K., & Rasmussen, J. J. 1991, J. Phys. Soc. Japan, 60, 735
Schmitz, H., Chapman, S. C., & Dendy, R. O. 2002, ApJ, 570, 637
Shimada, N., & Hoshino, M. 2000, ApJ, 543, L67